



**HAL**  
open science

## Discrete polynuclear manganese(ii) complexes with thiacalixarene ligands: synthesis, structures and photophysical properties

Yan Suffren, Niall O'Toole, Andreas Hauser, Erwann Jeanneau, Arnaud Brioude, Cedric Desroches

### ► To cite this version:

Yan Suffren, Niall O'Toole, Andreas Hauser, Erwann Jeanneau, Arnaud Brioude, et al.. Discrete polynuclear manganese(ii) complexes with thiacalixarene ligands: synthesis, structures and photophysical properties. Dalton Transactions, 2015, 44 (17), pp.7991-8000. 10.1039/c5dt00827a . hal-01597128

HAL Id: hal-01597128

<https://hal.science/hal-01597128>

Submitted on 16 May 2022

**HAL** is a multi-disciplinary open access archive for the deposit and dissemination of scientific research documents, whether they are published or not. The documents may come from teaching and research institutions in France or abroad, or from public or private research centers.

L'archive ouverte pluridisciplinaire **HAL**, est destinée au dépôt et à la diffusion de documents scientifiques de niveau recherche, publiés ou non, émanant des établissements d'enseignement et de recherche français ou étrangers, des laboratoires publics ou privés.



Distributed under a Creative Commons Attribution - NonCommercial 4.0 International License

# Discrete polynuclear manganese(II) complexes with thiacalixarene ligands: synthesis, structures and photophysical properties<sup>†</sup>

---

Yan Suffren,<sup>\*a</sup> Niall O'Toole,<sup>b</sup> Andreas Hauser,<sup>a</sup> Erwann Jeanneau,<sup>b</sup> Arnaud Brioude,<sup>b</sup> Cédric Desroches<sup>\*b</sup>

<sup>a</sup>*Département de chimie physique, Université de Genève, 30 Quai Ernest-Ansermet, 1211 Genève 4, Switzerland. E-mail: [Yan.Suffren@unige.ch](mailto:Yan.Suffren@unige.ch)*

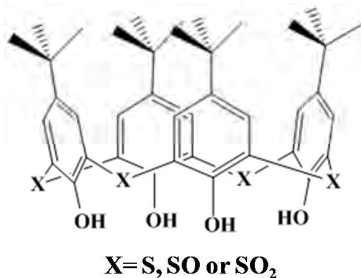
<sup>b</sup>*Laboratoire des Multimatériaux et Interfaces (UMR 5615), Université Claude Bernard de Lyon 1, Campus de la Doua, 69622 Villeurbanne, France. E-mail: [cedric.desroches@univ-lyon1.fr](mailto:cedric.desroches@univ-lyon1.fr)*

## Abstract

The synthesis, crystal structure and photophysical properties of the new compound  $[\text{Mn}_4(\text{ThiaSO}_2)_2\text{F}][\text{K}(18\text{-crown-6})]$ , ThiaSO<sub>2</sub> = *p*-*tert*butylsulphonylcalix[4]arene, are presented and compared to the ones of  $[\text{Mn}_4(\text{ThiaSO}_2)_2\text{F}]\text{K}$ . The strong orange luminescence is attributed to the  $\text{Mn}^{2+}$  centred  ${}^4\text{T}_1 \rightarrow {}^6\text{A}_1$  transition. Its temperature and pressure dependence and quenching by molecular dioxygen are reported. The latter is attributed to energy transfer from the  ${}^4\text{T}_1$  state exciting dioxygen to its  ${}^1\Sigma_g^+$  state. In the solid state, the quenching is much more efficient in  $[\text{Mn}_4(\text{ThiaSO}_2)_2\text{F}][\text{K}(18\text{-crown-6})]$  than in  $[\text{Mn}_4(\text{ThiaSO}_2)_2\text{F}]\text{K}$ . This is attributed to the open pore structure of the former allowing fast diffusion of dioxygen into the crystal lattice.

## Introduction

The macrocycle *p*-*tert*butylthiacalix[4]arene (ThiaS), a homologue of the calixarene family, consists of phenol moieties linked by sulphur atoms. Its ease of accessibility and strong multichelating power, arising from the proximity of the phenoxide groups to the bridging sulphur atoms, make this ligand a popular choice in coordination chemistry. Consequently, since the first synthesis of this molecule was described by the Myano group in 1997<sup>1</sup> (Scheme 1), a multitude of polynuclear metal complexes have been isolated, reinforcing: (i) its structuring role in the creation of either high-nuclearity isolable paramagnetic metal aggregates,<sup>2</sup> or the coordination-based molecular ‘building bricks’ leading to nano-capsule formation by supramolecular assembly,<sup>3</sup> and (ii) its electronic properties, known as the antenna effect, for luminescence in ions such as  $\text{Tb}^{3+}$  or even  $\text{Eu}^{3+}$ .<sup>4</sup>



**Scheme 1** Representation of *p*-*tert*butylthiacalix[4]arene (ThiaS with X = S), *p*-*tert*butylsulphoxycalix[4]arene (ThiaSO with X = SO) and *p*-*tert*butylsulphonylcalix[4]arene (ThiaSO<sub>2</sub> with X = SO<sub>2</sub>).

In previous work, we found that under solvothermal conditions *p-tert*butylthiacalix[4]arene and its sulphonyl and sulphoxide derivatives give rise to tetranuclear metallic complexes comprising  $\text{Mn}^{2+}$  ions. Differences in both the optical and structural properties were observed between those complexes obtained with ThiaS and ThiaSO,<sup>2d</sup> and those obtained with ThiaSO<sub>2</sub>.<sup>2k</sup> For ThiaS and ThiaSO neutral complexes are attained, consisting of two macrocycles and four  $\text{Mn}^{2+}$  ions in trigonal bipyramidal geometry. In both of these cases, no specific luminescence properties have been observed. For ThiaSO<sub>2</sub> a similar structure is obtained with the sole difference being the presence of a  $\mu_4\text{-OH}^-$  group at the centre of the square formed by the four  $\text{Mn}^{2+}$  ions, which display capped trigonal bipyramidal coordination geometry. This  $\mu_4\text{-OH}^-$  results in a negative charge over the aggregate, which is compensated by the presence of an alkali metal ion. In the solid state this ion interlinks the aggregates by ways of coordination to the oxygen atoms of sulphonyl groups. This family of clusters demonstrates an ambient temperature luminescence at a wavelength of approximately 580 nm when excited by illumination of 360 nm. Replacing the  $\mu_4\text{-OH}^-$  with  $\mu_4\text{-F}^-$  considerably increases the luminescence lifetime of this system.

The strong luminescence of the  $\text{Mn}^{2+}$  ion arising from  $^4\text{T}_1(^4\text{G})$  state was put to use at the start of the 20<sup>th</sup> century in luminescent mineral materials using red or green phosphors (neon discharge, fluorescent lamp).<sup>5</sup> Since then, intense spectroscopic studies have been carried out, which shed light on the importance of the environment of the  $\text{Mn}^{2+}$  ion as regards its luminescence properties.<sup>6</sup> However, despite the development of coordination chemistry, few studies have shown Mn(II) complexes presenting such properties at ambient temperature.<sup>7</sup> For this reason, we have resolved to pursue further investigation on the  $[\text{Mn}_4(\text{ThiaSO}_2)_2\text{F}]^-$  system by spectroscopic analysis, in both solution and the solid state. Moreover it has been shown that the conformation of the macrocycle, as well as the presence of sulphonyl groups, significantly modifies the electronic properties of the thiacalixarene family of complexes.<sup>8</sup>

Herein we report the preparation, crystal structures and photophysical behaviour of the new compound  $[\text{Mn}_4(\text{ThiaSO}_2)_2\text{F}][\text{K}(18\text{C}6)]$  (**2**), 18C6 = 18-crown-6, and compare the latter to the one

of  $[\text{Mn}_4(\text{ThiaSO}_2)_2\text{F}]\text{K}$  (**1**). We thus will study: (i) the effect of removing the  $\text{K}^+$ -sulphonyl interaction, and (ii) the effect of the conformation of the macrocycle.

## Results and discussion

### Crystal structure

The compounds of the tetranuclear complex **1** and **2** were obtained as pale-yellow coloured crystals with a relatively high yield by solvothermal reaction of  $\text{MnCl}_2 \cdot 4\text{H}_2\text{O}$ , p-tert-butylsulphonylcalix[4]arene ( $\text{ThiaSO}_2$ ) and KF for **1** and by adding 18C6 for **2** in a 1/10 (v/v)  $\text{H}_2\text{O}/\text{MeOH}$  mixed solvents (total 11 ml) at  $170^\circ\text{C}$  during at least 2 days.

Compounds **1** and **2** are composed of squares of four manganese (II) ions sandwiched between two  $\text{ThiaSO}_2$  macrocycles as shown in Fig. 1 and 2. In the middle of the square formed by the four manganese(II) ions, the presence of  $\mu_4\text{-F}^-$  gives a negative charge to the cluster. The electroneutrality of the complex is achieved by the presence of the  $\text{K}^+$  cation, coordinated by sulphonyl and methanol groups for **1** and coordinated by 18C6 and two methanol molecules for **2**. The originality of this type of aggregate, with a sevenfold  $[\text{MnO}_6\text{F}]$  coordination polyhedron having approximately  $\text{C}_{2v}$  symmetry and a square planar relationship to the fluoride group (Scheme 2), has already been discussed in a previous article.<sup>2k</sup> Both compounds crystallise in the  $P\bar{1}$  space group (for details of the structure determination see experimental section and Supporting Information).<sup>9</sup> For both, the centre of symmetry positioned on the fluoride group requires that the macrocycles, on either side of the square formed by the manganese ions, are crystallographically equivalent. The macrocycles of **1** and **2** are in a slightly distorted cone conformation: in **1**  $d(\text{O12} - \text{O33}) / d(\text{O27} - \text{O4}) = 0.98$  and in **2**  $d(\text{O4} - \text{O19}) / d(\text{O12} - \text{O30}) = 0.98$ .

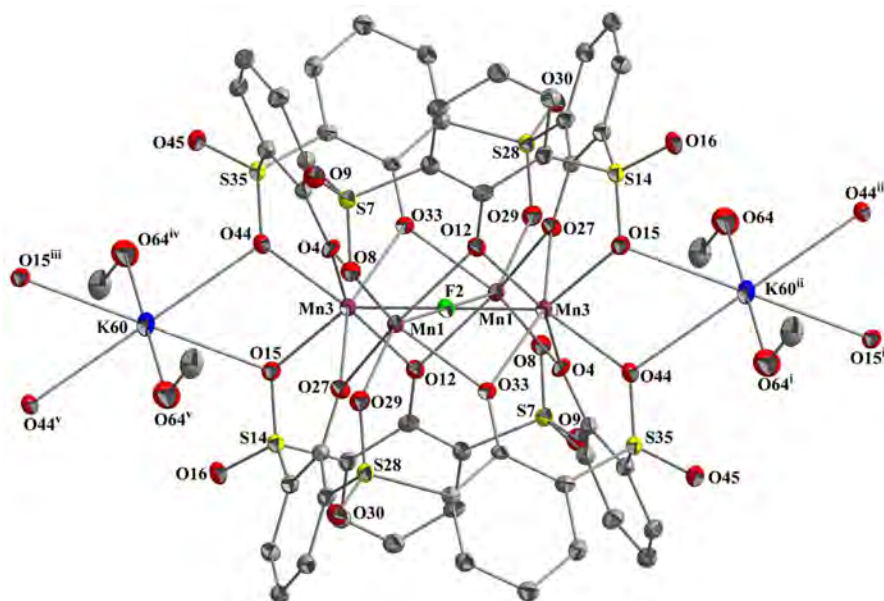


**Fig. 1** ORTEP<sup>10</sup> diagram of **1** with thermal ellipsoids at 50% probability. Hydrogen atoms and *tert*-butyl groups are omitted for clarity. Selected atom-atom distances [Å]: Mn1-Mn3<sup>i</sup> 3.0972(7); Mn1-F2 2.2018(5); F2-Mn3 2.1732(5); Mn1-O8 2.169(2) < Mn-O < Mn1-O4 2.242(2). Symmetry transformations used to generate equivalent atoms: <sup>i</sup> (1-x, 1-y, 1-z); <sup>ii</sup> (-1+x, y, z); <sup>iii</sup> (-3-x, 1-y, 1-z); <sup>iv</sup> (1+x, y, z); <sup>v</sup> (2-x, 1-y, 1-z).

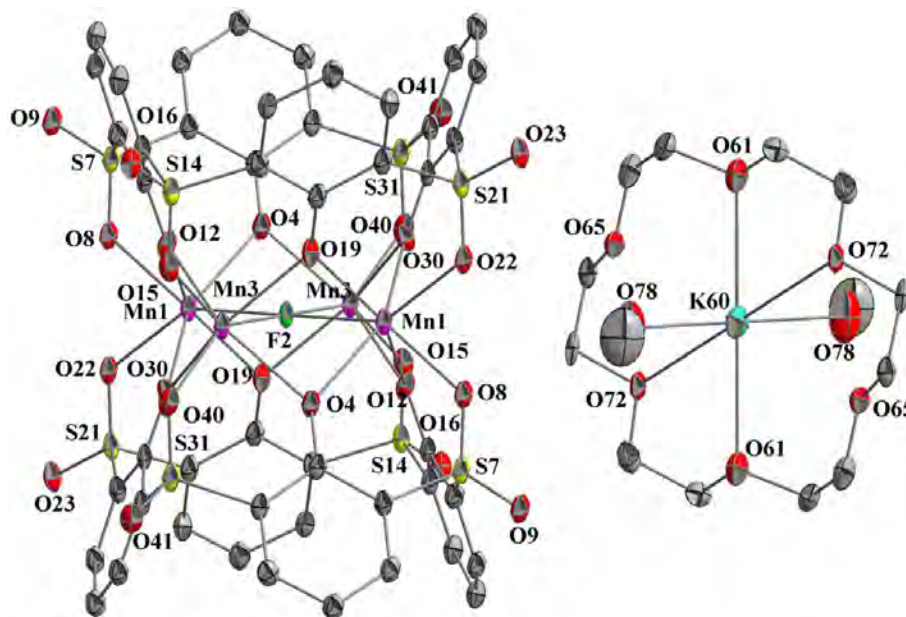
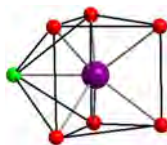


**Fig. 2** ORTEP<sup>10</sup> diagram of **2** with thermal ellipsoids at 50% probability. Hydrogen atoms and *tert*-butyl groups are omitted for clarity. Selected atom-atom distances [Å]: Mn1-F2 2.2091(4); Mn3-F2 2.1924(5); Mn1-Mn3 3.1057(7); Mn3-O15 2.177(2) < Mn-O < Mn3-O19<sup>i</sup> 2.247(2). Symmetry transformations used to generate equivalent atoms: <sup>i</sup> (-x+1, -y+1, -z+1); <sup>ii</sup> (-x, -y, -z+1); <sup>iii</sup> (-x+1, -y, -z+1); <sup>iv</sup> (x, y-1, z); <sup>v</sup> (-x, -y+1, -z+1).



**Scheme 2** Representation of the sevenfold  $[\text{MnO}_6\text{F}]$  coordination polyhedron having approximately  $C_{2v}$  symmetry.

The tetranuclear clusters in **1** are linked through the coordinated potassium ion and sulphonyl group, making **1** a one dimensional network (Fig. 3a). The coordination of  $\text{K}^+$  by the crown ether in **2** prevents interactions between the sulphonyl groups and the potassium ion. The tetranuclear clusters in **2** stack upon each other along the c-axis of the network, forming columns which are isolated from one another by the inclusion of  $[\text{K18C6}]^+$  groups (Fig. 3b). The shortest distance of the interaction between the  $\text{K}^+$  ion and the tetranuclear cluster in compound **1** is 2.72 Å (distance O15 – K60) whereas for compound **2** it is 5.54 Å (distance O8 – K60).

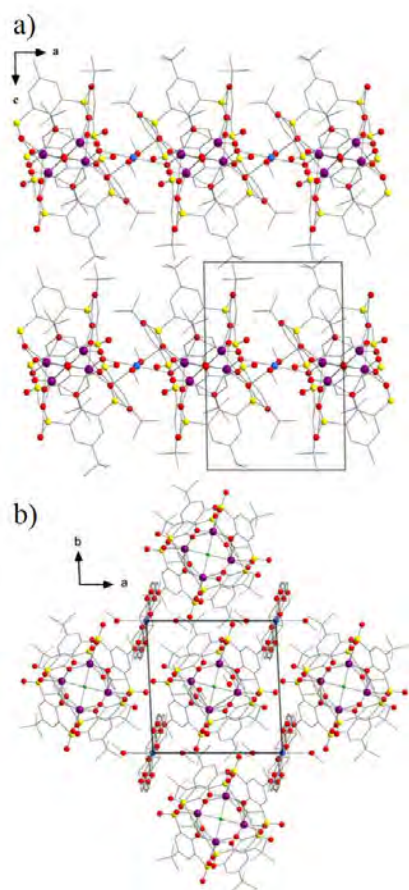


**Fig. 3 a)** Projection of the crystal packing of compound **1** in the (a, c) plane, **b)** projection of the crystal packing of compound **2** in the (a, b) plane.

### Photophysical characterisation

*Absorption and luminescence in DMF solution:* Fig. 4 shows the absorption, excitation and emission spectra at room temperature in dimethylformamide (DMF) solution of  $[\text{Mn}_4(\text{ThiaSO}_2)_2\text{F}]\text{K}$  (**1**) and  $[\text{Mn}_4(\text{ThiaSO}_2)_2\text{F}][\text{K}(18\text{C}6)]$  (**2**) between 11000 and 38000  $\text{cm}^{-1}$  (265 - 910 nm). The absorption spectrum of **1** is identical to that of **2**. The absorption bands observed are mainly the signature of the ThiaSO<sub>2</sub> calixarene ligand. In the UV region there are two band maxima  $\tilde{\nu}_{\text{max}1}$  and  $\tilde{\nu}_{\text{max}2}$  at 28490  $\text{cm}^{-1}$  (351 nm) and 35300  $\text{cm}^{-1}$  (283 nm), respectively. These two bands can be attributed to  $\pi \rightarrow \pi^*$  transitions of the ThiaSO<sub>2</sub> ligand. The molar extinction coefficient of the intense absorption band at 28490  $\text{cm}^{-1}$  is within experimental accuracy identical for the two compounds with a value of  $\epsilon_{\text{max}} = 72000 \text{ M}^{-1}\text{cm}^{-1}$ .

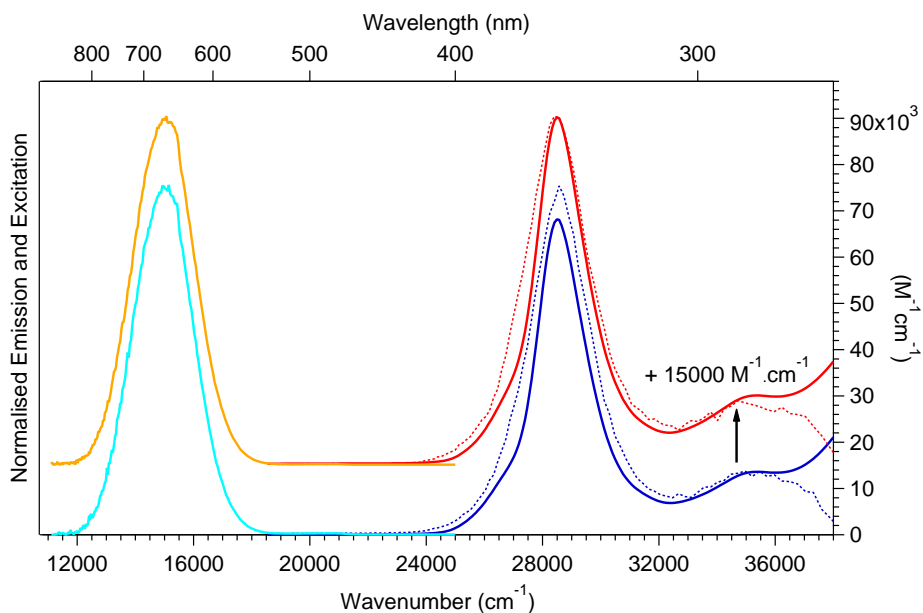


**Fig. 4** Absorption (red and dark blue curves), excitation (red and blue dotted curves) and emission (orange and light blue curves) spectra in DMF solution of  $[\text{Mn}_4(\text{ThiaSO}_2)_2\text{F}]\text{K}$  **1** and  $[\text{Mn}_4(\text{ThiaSO}_2)_2\text{F}][\text{K}(18\text{C}6)]$  **2** at room temperature,  $c = 1.5 \times 10^{-4} \text{ M}$  for **1** and  $c = 1.2 \times 10^{-4} \text{ M}$  for **2** for the absorption and emission spectra, and  $c = 1.5 \times 10^{-6} \text{ M}$  for **1** and  $c = 1.3 \times 10^{-6} \text{ M}$  for **2** for the excitation spectra. The spectra of **2** are offset along the intensity/absorptivity axes for clarity.

The emission spectra of **1** and **2** in DMF (see Fig. 4) upon photoexcitation at 28570  $\text{cm}^{-1}$  (350 nm) show an intense and broad luminescence band between 12000 and 18000  $\text{cm}^{-1}$  (555 - 833

nm) with a maximum  $\tilde{\nu}_{\max}$  at  $15010\text{ cm}^{-1}$  (666 nm). As expected, in solution the influence of the cation is negligible and no difference in the emission spectra between the two compounds has been observed. The orange-red luminescence with a very large gap between the strong absorption at  $28490\text{ cm}^{-1}$ , a lifetime of  $35\text{ }\mu\text{s}$  and a quantum efficiency of 0.4% in non-deoxygenated solution at 298 K (compared to 1.08 ms and therefore around 15% in a deoxygenated solution) originates from the lowest energy component of the  ${}^4\text{T}_1(\text{t}_{2\text{g}}^4\text{e}_{\text{g}}^1) \rightarrow {}^6\text{A}_1(\text{t}_{2\text{g}}^3\text{e}_{\text{g}}^2)$  d-d transition of the manganese(II) ions in  $\text{d}^5$  high-spin configuration. As mentioned above, the crystal structure reveals a sevenfold coordination sphere for the Mn(II) ions in a monocapped trigonal prism geometry and close to  $\text{C}_{2\text{v}}$  symmetry, resulting in a large splitting of the  ${}^4\text{T}_1$  state of octahedral parentage (see below). In essence, photoexcitation into the ligand centred  $\pi\text{-}\pi^*$  transition at  $28570\text{ cm}^{-1}$  is followed by fast intersystem crossing and internal conversion, thus resulting in the orange-red metal-centred d-d luminescence.

The above is further borne out by the excitation spectra of both compounds in DMF solution included in Fig. 4, which were collected at the emission maximum of  $15380\text{ cm}^{-1}$  (650 nm) and at very low concentrations of  $c = 1.5 \times 10^{-6}\text{ M}$  in order to minimise saturation effects in the region of the strong UV absorption bands. They are indeed perfectly superimposed to the absorption spectra thus proving unambiguously that the emission is intrinsic to the complexes.

*Solid-state emission and excitation spectra:* The low temperature solid-state emission and excitation spectra for the compounds **1** and **2** are displayed in Fig. 5. Upon excitation at  $28570\text{ cm}^{-1}$  (350 nm), **1** presents an intense broad and asymmetric emission band centred at  $16600\text{ cm}^{-1}$  (602 nm) with a full width at half maximum (FWHM) of approximately  $1700\text{ cm}^{-1}$ . In contrast, **2** shows an intense symmetric emission band at  $15660\text{ cm}^{-1}$  (639 nm) and a FWHM of about  $2000\text{ cm}^{-1}$ . Thus there is a redshift of the luminescence band maximum by around  $950\text{ cm}^{-1}$  and an increase by about 18% of the FWHM between compounds **1** and **2**. As in solution, the orange-red luminescence band originates from the  ${}^4\text{T}_1 \rightarrow {}^6\text{A}_1$  transition of the Mn(II) in  $\text{d}^5$  high-spin configuration.

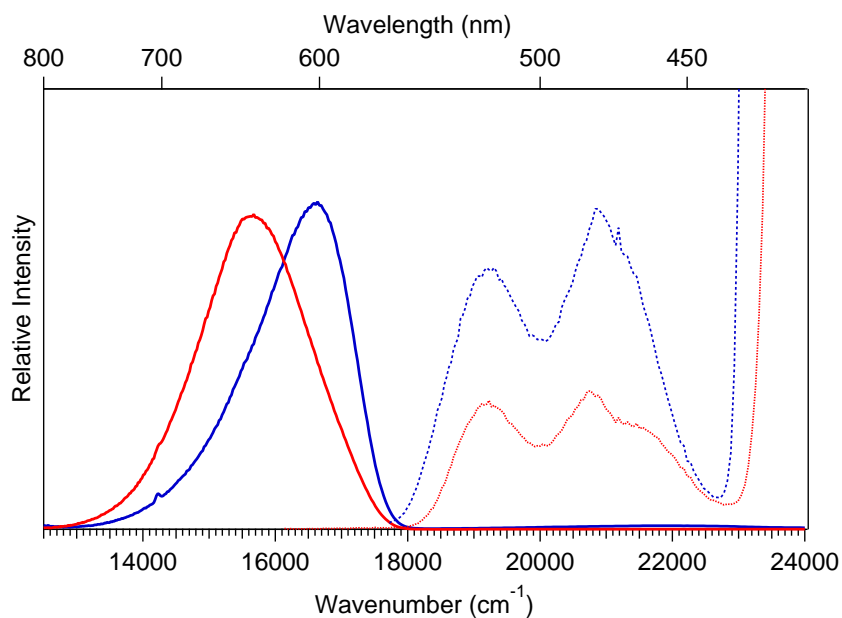


**Fig. 5** Solid-state emission spectra (solid curves) at 7.5 K upon photoexcitation at  $28570\text{ cm}^{-1}$  (350 nm) and excitation spectra at 8 K (dotted curves) of  $[\text{Mn}_4(\text{ThiaSO}_2)_2\text{F}]\text{K}$  **1** (blue) and  $[\text{Mn}_4(\text{ThiaSO}_2)_2\text{F}][\text{K}(18\text{C}6)]$  **2** (red).

The solid-state excitation spectra at 8 K for both compounds are included in Fig. 5. In the UV region of the strong ligand-centred  $\pi\text{-}\pi^*$  absorption bands they are saturated. However, they show a broad and structured band with two maxima  $\tilde{\nu}_{\text{max}1}$  and  $\tilde{\nu}_{\text{max}2}$  localised at approximately  $19200\text{ cm}^{-1}$  (521 nm) and  $20800\text{ cm}^{-1}$  (481 nm), respectively, and an indication of a shoulder on the high-energy side. These can be attributed to the split components of the d-d  ${}^6\text{A}_1 \rightarrow {}^4\text{T}_1$  transition of the manganese(II) ion, as in  $\text{C}_{2v}$  the excited  ${}^4\text{T}_1$  state is split into three energy level in first order.

*Temperature-dependence of the  $\text{Mn}^{2+}$  luminescence:* The luminescence of **1** and **2** in the solid state between 7.5 K and room temperature and in vacuum on excitation at  $28570\text{ cm}^{-1}$  (350 nm) is shown in Fig. 6. The luminescence intensity of **1** decreases only slightly as temperature increases up to just below room temperature and then drops more rapidly to 70% of its low-temperature value, as shown in Fig. 7. At the same time the FWHM increases by 29%, that is, from  $1700$  to  $2200\text{ cm}^{-1}$ , whereas the band maximum  $\tilde{\nu}_{\text{max}}$  is stable between 7.5 and 100 K with a value of  $16600\text{ cm}^{-1}$ , and shifts to slightly higher energies above 100 K.

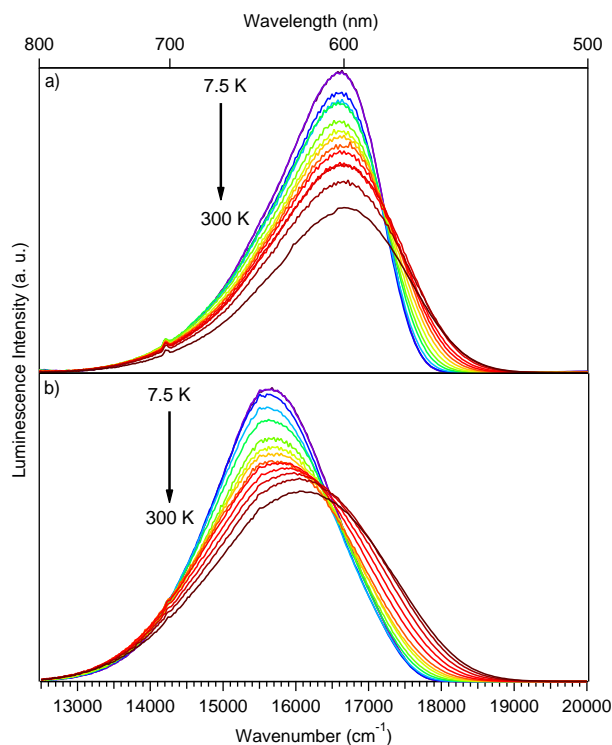


**Fig. 6** Solid-state emission spectra of  $[\text{Mn}_4(\text{ThiaSO}_2)_2\text{F}]\text{K}$  **1** (a) and  $[\text{Mn}_4(\text{ThiaSO}_2)_2\text{F}][\text{K}(18\text{C}6)]$  **2** (b) between 7.5 and 300 K upon photoexcitation at  $28570\text{ cm}^{-1}$  (350 nm).

For **2** the luminescence shows the same temperature dependence as for **1** with a somewhat smaller decrease to 88% between 7.5 and 300 K. The variation of the FWHM is slightly larger for **2** than for **1**, with an increase by approximately 39% from  $2000\text{ cm}^{-1}$  to  $2780\text{ cm}^{-1}$  in the same temperature range, and a slight redshift from  $15660$  to  $15630\text{ cm}^{-1}$  between 7.5 and 25 K followed by a blueshift to  $16090\text{ cm}^{-1}$  is observed for **2**. At a given temperature, the FWHM for **2** is larger than for **1**.

Fig. 7b includes the luminescence lifetimes for **1** and **2** between 3 K and 300 K under pulsed photoexcitation at  $28170\text{ cm}^{-1}$  (355 nm). Decay curves are close to single exponential except for a small deviation at short times. At 3 K the lifetimes calculated by the Igor fitting software<sup>11</sup> are 2.12 ms for **1** and 2.31 ms for **2**, respectively. They increase between 3 K and 75 K for **1** with a maximum value of 2.41 ms and between 3 K and 100 K for **2** with a maximum value of 2.48 ms. Then, the lifetime values decrease gradually up to room temperature reaching 1.65 ms and 2.00 ms for **1** and **2**, respectively. The luminescence quantum yield for **1** in the solid state at room

temperature is around 50%. Together with the above luminescence lifetime this gives a radiative lifetime of around 3 ms, which is typical for spin-forbidden d-d transitions.

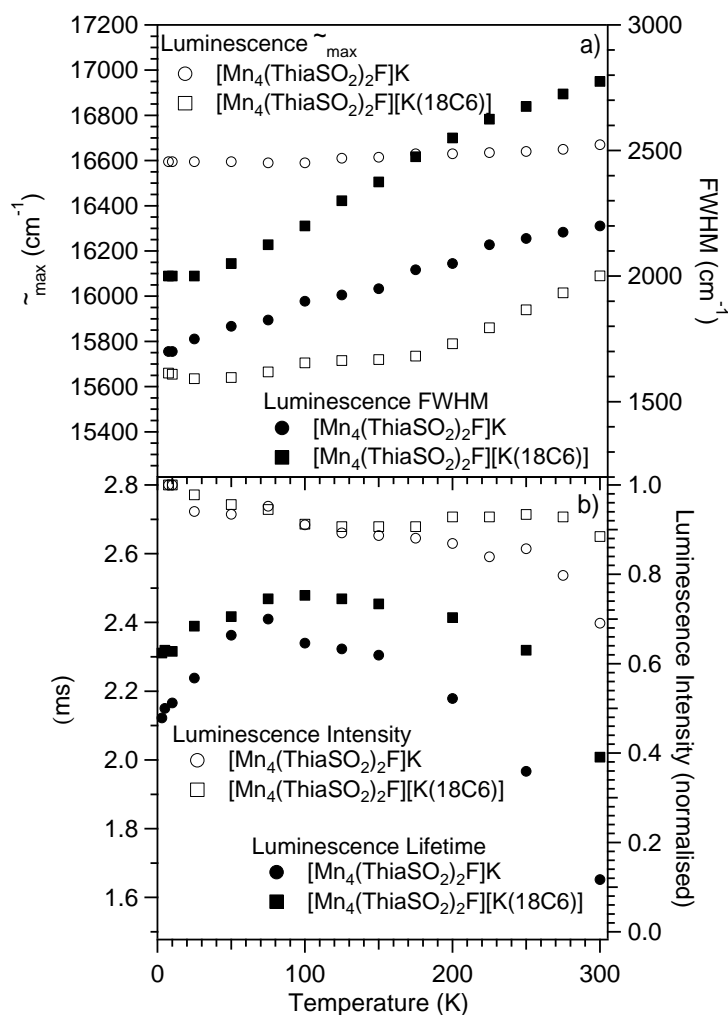


**Fig. 7** a) The energy band maxima  $\tilde{\nu}_{\max}$  (left axis) and FWHM (right axis) upon photoexcitation at  $28570 \text{ cm}^{-1}$  (350 nm) of **1** (circles) and **2** (squares). b) Luminescence lifetimes (left axis) and integrated luminescence intensities (right axis) of **1** (circles) and **2** (squares) as function of temperature. The luminescence lifetimes and intensities are obtained upon photoexcitation at  $28170 \text{ cm}^{-1}$  (355 nm, pulsed laser) and  $28570 \text{ cm}^{-1}$  (350 nm, continuous laser), respectively.

*O<sub>2</sub> pressure-dependence of the Mn<sup>2+</sup> luminescence–quenching in the solid state:* As mentioned above, in solution the presence of oxygen quenches the Mn<sup>2+</sup> luminescence considerably, such that in a deoxygenated solution at room temperature the luminescence quantum efficiency is around 15% whereas under atmospheric conditions it is only 0.4%. What about the influence of O<sub>2</sub> on the solid-state luminescence? Fig. 8 shows the luminescence spectra of **1** and **2** at 298 K as a function

of the air pressure between 0.1 and 1010 mbar. The behaviour observed is reversible and reproducible. The luminescence intensities increase and decrease within a few seconds by removing from or introducing the O<sub>2</sub> into the sample compartment.

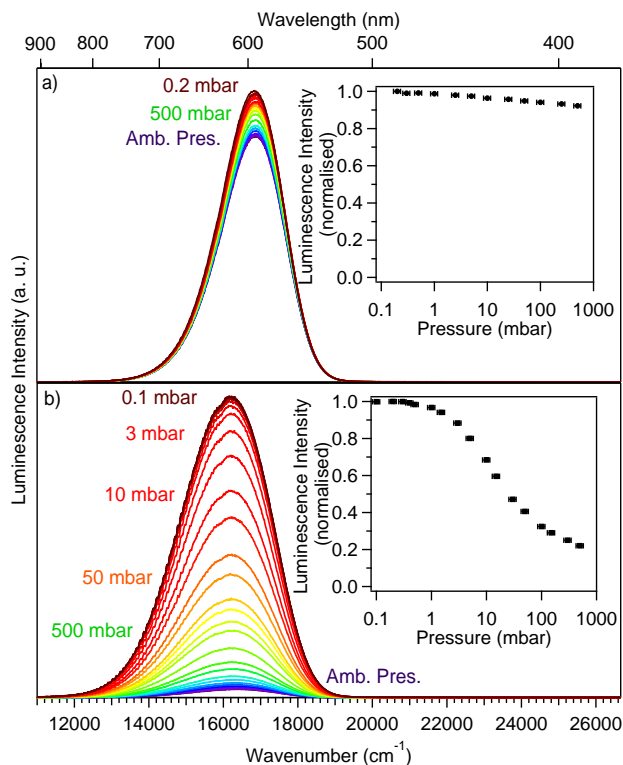


**Fig. 8** Solid-state emission spectra of [Mn<sub>4</sub>(ThiaSO<sub>2</sub>)<sub>2</sub>F]K **1** (a) and [Mn<sub>4</sub>(ThiaSO<sub>2</sub>)<sub>2</sub>F][K(18C6)] **2** (b) at variable molecular oxygen pressure and upon photoexcitation at 24690 cm<sup>-1</sup> (405 nm). The normalised luminescence intensities are plotted in the top and bottom insets for **1** and **2**, respectively.

For **1**, the luminescence intensity decreases only by approximately 15% between 0.1 and 1010 mbar. For **2**, the intensity decreases quite rapidly to less than 5% of its initial value. The difference in behaviour between the two compounds must be due to the structural differences. In **1**, the K<sup>+</sup> cations bridge the [Mn<sub>4</sub>(ThiaSO<sub>2</sub>)<sub>2</sub>F]<sup>-</sup> entities leading to compact structure limiting the diffusion of the dioxygen into the lattice. In contrast, for **2** the isolated [K(18C6)]<sup>+</sup> cations create a porous structure with empty spaces between the [Mn<sub>4</sub>(ThiaSO<sub>2</sub>)<sub>2</sub>F]<sup>-</sup> entities connected only by weak ionic interactions. The dioxygen can be removed or introduced more easily into the structure.

The most probable mechanism for the quenching of the spin-forbidden  $\text{Mn}^{2+}$  centred  ${}^4\text{T}_1 \rightarrow {}^6\text{A}_1$  luminescence is given by a spin-conserving energy transfer process from the excited complex to  $\text{O}_2$  thereby exciting  $\text{O}_2$  from its  ${}^3\Sigma_g^-$  ground state to the excited  ${}^1\Sigma_g^+$  state.<sup>12</sup>

For comparison to the solid state, the  $\text{O}_2$  pressure-dependence of the luminescence behaviour was studied for the two compounds in DMF solution where the  $[\text{Mn}_4(\text{ThiaSO}_2)_2\text{F}]^-$  tetranuclear complex is considered as totally isolated. The luminescence spectra of solutions of **1** and **2** after different times (0 – 900 s) of de-oxygenation by  $\text{N}_2$  bubbling were recorded (see Fig. S1 and S2 in Supporting Information). The reversibility was checked as function of time (0 – 3600 s) of re-oxygenation of the  $\text{N}_2$  saturated solution by exposing them to air (see Fig. S3 and S4 in Supporting Information). As for the solids, the luminescence behaviour is reversible, with an increase and a decrease of the luminescence intensities by bubbling  $\text{N}_2$  (removal  $\text{O}_2$ ) and by re-oxygenation (exposing to air), respectively. The maximum luminescence intensities are observed after approximately 120 s of  $\text{N}_2$  bubbling (see Fig. S5 in Supporting Information).

*Pressure-dependence of the  $\text{Mn}^{2+}$  luminescence:* Fig. 9a and 9b show the luminescence spectra of **1** and **2**, respectively, between ambient pressure and 10 GPa at room temperature. In addition to the broad band due the  $\text{Mn}^{2+}$  luminescence, all show a series of sharp bands corresponding to  $\text{BaFCl}:\text{Sm}^{2+}$  f-f luminescence introduced into diamond anvil cell (DAC) as in situ pressure sensor.<sup>13</sup>

For **1** the luminescence intensity increases by approximately 10% between ambient pressure and 0.3 GPa, then it decreases gradually and becomes very weak at a pressure of 9.6 GPa. At the same time the luminescence band maximum shifts linearly to lower energies by  $-230 \text{ cm}^{-1}/\text{GPa}$  (Fig. 10a). For **2**, the behaviour at variable pressure is very similar to **1**, except that the initial increase in intensity up to a pressure of 0.4 GPa is much larger. The luminescence band maximum is stable up to this pressure, above that pressure it likewise shifts to the red by  $-190 \text{ cm}^{-1}/\text{GPa}$ , that is, close to the value obtained for compound **1** (Fig. 10a). Such a redshift is expected for the spin-forbidden  ${}^4\text{T}_1(t_{2g}^4 e_g^1) \rightarrow {}^6\text{A}_1(t_{2g}^3 e_g^2)$  d-d transition. The formal transfer of an electron from a non-bonding  $t_{2g}$

orbital to an anti-bonding  $e_g$  orbital results in an expansion of the coordination sphere during the emission process. Thus external pressure destabilises the ground state with respect to the first excited state by a work term of the form  $p\Delta V$ .<sup>14</sup> The shift of around  $-200 \text{ cm}^{-1}/\text{GPa}$  corresponds to  $\Delta V \approx 5 \text{ \AA}^3/\text{complex}$ . This is in line with ligand-field theoretical considerations. As pressure increases, the Mn-O bond is slightly compressed and therefore the ligand-field strength increases. According to the Tanabe-Sugano diagram<sup>15</sup> for  $d^5$  this results in a decrease of the energy of the  ${}^4T_1$  state with respect to the  ${}^6A_1$  ground state.

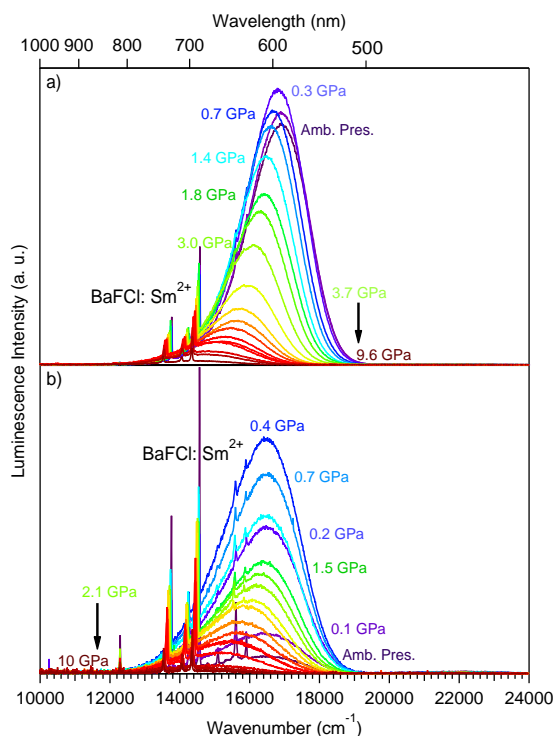


**Fig. 9** Solid-state emission spectra of  $[\text{Mn}_4(\text{ThiaSO}_2)_2\text{F}]\text{K}$  **1** (a) and  $[\text{Mn}_4(\text{ThiaSO}_2)_2\text{F}][\text{K}(18\text{C}6)]$  **2** (b) between ambient pressure and 10 GPa upon photoexcitation at  $24690 \text{ cm}^{-1}$  (405 nm) at 298 K. The pressure in the DAC has been determined by following the shift of the  ${}^5D_0 \rightarrow {}^7F_0$  emission band of the samarium(II) ion in BaFCl:Sm<sup>2+</sup> compound (room temperature rate of  $-21 \text{ cm}^{-1}/\text{GPa}$ ).<sup>13</sup>

The luminescence lifetimes between ambient pressure and 10 GPa and are plotted in Fig. 10b. For **1**, the lifetime at ambient pressure in the DAC is 1.71 ms. This value is in line with the values of 1.65 and 1.68 ms determined for **1** in the presence and absence of atmospheric  $\text{O}_2$ ,

respectively. As pressure increases, the lifetime decreases continuously from 1.71 ms to 0.55 ms. Concomitantly, the luminescence intensity decreases likewise with increasing pressure.

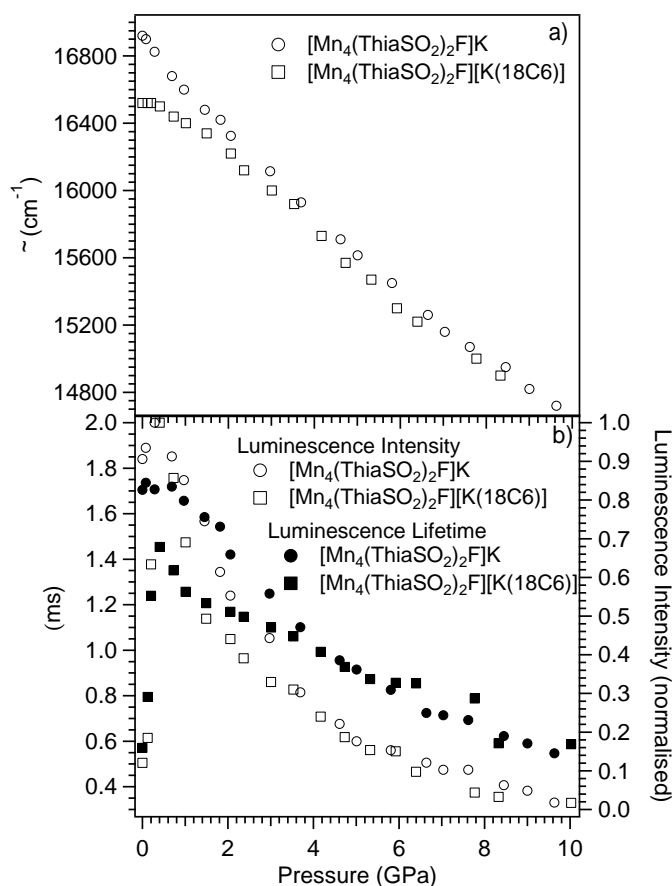


**Fig. 10** a) The energy band maxima  $\tilde{\nu}_{\max}$  upon photoexcitation at  $24690\text{ cm}^{-1}$  (405 nm) of **1** (circles) and **2** (squares). b) Luminescence lifetimes (left axis) and integrated luminescence intensities (right axis) of **1** (circles) and **2** (squares) as function of pressure. The luminescence lifetimes and intensities at 298 K were obtained upon photoexcitation at  $28170\text{ cm}^{-1}$  (355 nm, pulsed laser) and  $24690\text{ cm}^{-1}$  (405 nm, continuous laser) respectively.

For **2**, the luminescence lifetime of 0.57 ms at ambient pressure in the DAC is lower than the lifetime of 2.00 ms measured at room temperature and ambient pressure in a helium gas medium. Indeed, the value of 0.57 ms for the luminescence lifetime in the DAC is close to the value of 0.53 ms in the solid state under atmospheric pressure, thus indicating that oxygen also quenches the luminescence in the sample prepared in the DAC. The luminescence lifetime for **2** then first increases from 0.57 ms at ambient pressure to 1.45 ms at 0.4 GPa, then it gradually decreases at

higher pressure to 0.59 ms at 9.6 GPa, that is, above 0.4 GPa it shows the same behaviour as for compound **1**. Likewise the luminescence intensity increases up to 0.4 GPa and then decreases concomitantly with the lifetime. The strong increase of the luminescence lifetime and intensity between ambient pressure and 0.4 GPa is unusual. The only possible reason to explain this behaviour is that the O<sub>2</sub> that has diffused into the lattice at ambient pressure is almost quantitatively expelled from lattice upon application of a comparatively low pressure, thus reducing the quenching of the Mn<sup>2+</sup>.

The decrease in luminescence lifetime and intensity with increasing pressure for **1** right from the beginning and for **2** for pressures above 0.4 GPa indicates a gradual decrease in luminescence quantum efficiency. Such a decrease is expected based on the energy gap law<sup>16</sup> which states that the non-radiative decay rate constant increases exponentially with a decreasing zero-point energy difference. Quantitatively, according to the decrease in lifetime the quantum efficiency should decrease from the maximum value of 50% at ambient pressure and room temperature to around 15% at 10 GPa. However, the actual luminescence intensity at 10 GPa is less than 5% of its maximum value. The reason for this apparent discrepancy is not entirely clear. It seems to indicate that concomitantly with the increase in the non-radiative decay rate constant the radiative lifetime increases. This could be related to the fact that the lowest excited state of Mn<sup>2+</sup> consists of a multiplet with components in thermal equilibrium having different radiative lifetimes and luminescence quantum efficiencies. Pressure would then not only shift the energy of this multiplet with respect to the ground state, but also influence the multiplet splittings and thus the observed lifetime and luminescence quantum efficiencies differently.

## Conclusions

Thiacalixarene complexes have been studied since the late 1990's for their magnetic, electronic and optical properties, with various potential applications such as molecular recognition, catalysis, self-assembly, and nanomedicine.<sup>17</sup> The new calixarene compound, [Mn<sub>4</sub>(ThiaSO<sub>2</sub>)<sub>2</sub>F][K(18C6)] has

been characterised by single crystal X-ray diffraction. The structural studies reveal a structure very similar to that of  $[\text{Mn}_4(\text{ThiaSO}_2)_2\text{F}]\text{K}$ , with a square of four manganese(II) ions sandwiched between two ThiaSO<sub>2</sub> macrocycles. The main difference between the two structures lies in the connection of the tetranuclear clusters in the form of a one dimensional network of the clusters for **1** by  $\text{K}^+$  coordination, and to isolated clusters by the inclusion of  $[\text{K18C6}]^+$  for **2**. In both clusters, the manganese  $\text{C}_{2v}$  symmetry and the  $\mu_4\text{-F}^-$  square planar geometry are rare examples in the literature. Both compounds present an intense and broad luminescence band originating from the  ${}^4\text{T}_1(\text{t}_2\text{g}^4\text{e}_\text{g}^1) \rightarrow {}^6\text{A}_1(\text{t}_2\text{g}^3\text{e}_\text{g}^2)$  d-d transition of the manganese(II) ions. This luminescence has been studied at variable temperature and ambient pressure as well as at variable pressure at room temperature. The presence of oxygen in solution and in the solid state quenches the  $\text{Mn}^{2+}$  luminescence by energy transfer from the excited complex to  $\text{O}_2$  thereby exciting  $\text{O}_2$  from its  ${}^3\Sigma_\text{g}^-$  ground state to the excited  ${}^1\Sigma_\text{g}^+$  state. The quenching is more efficient for the  $[\text{K(18C6)}]^+$  containing compound with its open structure, which facilitates  $\text{O}_2$  diffusion into the lattice. This is the first compound of a calixarene complex showing such a strong  $\text{O}_2$  pressure dependence in the solid state. Interestingly, a comparatively low hydrostatic pressure squeezes out the  $\text{O}_2$ , thus restoring the luminescence intensity.

## Experimental

All chemicals and solvents were used as received (solvents: Carlo Erba RPE; chemicals: Aldrich); all preparations and manipulations were performed under aerobic conditions. The ligands, p-tert-butylthiacalix[4]arene (ThiaS)<sup>1a,18</sup>, p-tert-butylsulphonylcalix-[4]arene (ThiaSO<sub>2</sub>)<sup>2a,19</sup> and compound **1**<sup>2k</sup> were synthesised by the published procedures. FT-IR spectra were recorded on a Nicolet 380 spectrometer. Mass spectra were performed on a MicroTOF-QII Bruker mass spectrometer (ESI Source).

**Synthesis of  $[\text{Mn}_4(\text{ThiaSO}_2)_2(\text{F})][\text{K(18C6)}]\cdot 2\text{CH}_3\text{OH}$  (**2**).** Compound **2** was obtained in the form of pale-yellow coloured crystals from the reaction mixture of p-tertbutylsulphonylcalix[4]arene

(ThiaSO<sub>2</sub>) (0.05 g, 0.059 mmol) with MnCl<sub>2</sub>·4H<sub>2</sub>O (0.05 g, 0.252 mmol), KF (0.02 g, 0.357 mmol), 18-crown-6 (0.02g, 0.075 mmol), methanol (10 mL) and water (1 ml) in a 23 mL Teflon-lined autoclave under an autogenous pressure at 170°C for 3 days. The crystals were isolated upon filtration and were washed with methanol. Yield: 60%. IR (cm<sup>-1</sup>) MS ESI (negative mode): [(Mn<sub>4</sub>(ThiaSO<sub>2</sub>)<sub>2</sub>F)] calculated: 1927m/z, found: 1927,03m/z.

**Single Crystal X-Ray Diffraction XRD.** Suitable crystals were selected and mounted on a Gemini kappa-geometry diffractometer (Agilent Technologies UK Ltd) equipped with an Atlas CCD detector and using Mo radiation ( $\lambda = 0.71073 \text{ \AA}$ ). Intensities were collected at 100 K by means of the CrysAlisPro software.<sup>20</sup> Reflection indexing, unit-cell parameters refinement, Lorentz- polarisation correction, peak integration and background determination were carried out with the CrysAlisPro software.<sup>20</sup> An analytical absorption correction was applied using the modeled faces of the crystal.<sup>21</sup> The structures were solved by direct methods with SIR97 and the least-square refinement on F<sup>2</sup> was achieved with the CRYSTALIS software.<sup>22</sup> All non-hydrogen atoms were refined anisotropically. The hydrogen atoms were all located in a difference map, but those attached to carbon atoms were repositioned geometrically. The H atoms were initially refined with soft restraints on the bond lengths and angles to regularise their geometry (C-H in the range 0.93 - 0.98 Å, N-H in the range 0.86 - 0.89 Å and O-H = 0.82 Å, and Uiso(H) in the range 1.2 - 1.5 times Ueq of the parent atom), after which the positions were refined with riding constraints. For the experimental details see supporting information. CCDC-1050380 contain the supplementary crystallographic data for this paper. These may be obtained free of charge from The Cambridge Crystallographic Data Centre via [www.ccdc.cam.ac.uk/data\\_request/cif](http://www.ccdc.cam.ac.uk/data_request/cif).

**Spectroscopic Measurements.** Electronic absorption spectra in the UV-Vis were recorded at 293 K from solutions in dimethylformamide (DMF) with a double beam absorption spectrometer (Agilent, Cary 5000) and a commercial fluorimeter (Jobin Yvon Horiba FL3-22, Fluorolog®-3) equipped with a peltier-cooled photomultiplier (Hamamatsu R2658P, sensitivity: 185 – 1010 nm) using quartz cells of 0.2 cm and 1 cm path length, for the absorption, and excitation-emission spectra,

respectively. Powder samples were mounted directly onto copper plates using conductive silver glue and cooled in an optical closed-cycle cryostat capable of reaching temperatures down to 3 K in a helium atmosphere (*Sumitomo SHI-950/Janis Research CCS-500/204*). The emission spectra at variable temperature (7.5 – 293 K) were measured on the *Fluorolog®-3* spectrometer. High resolution emission spectra were recorded upon excitation with 405 and 473 nm diode lasers or with a Nd:YAG laser (*Quantel Brilliant B*) using the third harmonic at 355 nm. The emitted light was analysed at 90° with a *Spex 270M* monochromator with holographic gratings (150 grooves/mm, blazed at 600). Light intensity was detected by a photomultiplier (Hamamatsu R928) or CCD camera. Appropriate filters were utilised to remove the laser light, the Rayleigh scattered light and associated harmonics from the emission spectra. The emission spectra were corrected for the instrumental response function. Luminescent lifetimes were measured using the excitation provided by the third harmonic of the Nd:YAG. The output signal of the photomultiplier was fed into a multichannel scaler (*Stanford Research SR-400*) and transferred to a PC for data analysis. Lifetimes were averages of 3 independent determinations. The spectra were displayed as photons versus energy ( $\text{cm}^{-1}$ ) on the bottom axis and versus wavelength (nm) on the top axis. Luminescence spectra under high pressure were recorded using a diamond anvil cell (MiniDAC of D'Anvils Ltd.), which could also be inserted into the closed cycle cryostat. Pressure was calibrated by using the  $^5\text{D}_0 \rightarrow ^7\text{F}_0$  luminescence of  $\text{Sm}^{2+}$  doped BaFCl with a shift rate of  $-21 \text{ cm}^{-1}\text{GPa}^{-1}$  as internal pressure sensor.<sup>13</sup> The air pressure-dependent solid-state luminescence spectra have been realised in a cryostat equipped with a primary pump and an APG100 active Pirani vacuum gauge (*Edwards*). The degassed solutions were realised in a 1 cm corked cuvette with a Schlenk line equipped with a small Teflon-PTFE tube provided of a medical needle, and a  $\text{N}_2$  bottle. The re-oxygenation of the solution were realised by removing the plug from the cuvette and leaving it open to ambient air. Spectra were recorded on the *Fluorolog®-3* spectrometer with different times of  $\text{N}_2$  bubbling (0 – 900 seconds) and  $\text{O}_2$  re-oxygenation (0 – 60 minutes).

## Acknowledgements

We thank the Swiss National Science Foundation (grant number 200020\_152780) for financial support.

## References

- 1 (a) H. Kumagai, M. Hasegawa, S. Miyanari, Y. Sugawa, Y. Sato, T. Hori, S. Ueda, H. Kamiyama and S. Miyano, *Tetrahedron Lett.*, 1997, **38**, 3971-3972; (b) T. Kajiwara, N. Iki and M. Yamashita, *Coord. Chem. Rev.*, 2007, **251**, 1734-1746.
- 2 (a) G. Mislin, E. Graf, M. W. Hosseini, A. Bilyk, A. K. Hall, J. M. Harrowfield, B. W. Skelton and A. H. White, *Chem. Commun.*, 1999, 373-374; (b) T. Kajiwara, S. Yokozawa, T. Ito, N. Iki, N. Morohashi and S. Miyano, *Chem. Lett.*, 2001, 6-7; (c) H. Akdas, E. Graf, M. W. Hosseini, A. De Cian, A. Bilyk, B. W. Skelton, G. A. Koutsantonis, I. Murray, J. M. Harrowfield and A. H. White, *Chem. Commun.*, 2002, 1042-1043; (d) C. Desroches, G. Pilet, S. A. Borshch, S. Parola and D. Luneau, *Inorg. Chem.*, 2005, **44**, 9112-9120; (e) C. Desroches, G. Pilet, P. A. Szilagy, G. Molnar, S. A. Borshch, A. Bousseksou, S. Parola and D. Luneau, *Eur. J. Inorg. Chem.*, 2006, 357-365; (f) T. Kajiwara, T. Kobashi, R. Shinagawa, T. Ito, S. Takaishi, M. Yamashita and N. Iki, *Eur. J. Inorg. Chem.*, 2006, 1765-1770; (g) Y. Bi, X.-T. Wang, W. Liao, X. Wang, X. Wang, H. Zhang and S. Gao, *J. Am. Chem. Soc.*, 2009, **131**, 11650-11651; (h) Y. Bi, W. Liao, G. Xu, R. Deng, M. Wang, Z. Wu, S. Gao and H. Zhang, *Inorg. Chem.*, 2010, **49**, 7735-7740; (i) Y. Bi, S. Du and W. Liao, *Chem. Commun.*, 2011, **47**, 4724-4726; (j) A. Gehin, S. Ferlay, J. M. Harrowfield, D. Fenske, N. Kyritsakas and M. W. Hosseini, *Inorg. Chem.*, 2012, **51**, 5481-5486; (k) M. Lamouchi, E. Jeanneau, A. Pillonnet, A. Brioude, M. Martini, O. Stephan, F. Meganem, G. Novitchi, D. Luneau and C. Desroches, *Dalton Trans.*, 2012, **41**, 2707-2713; (l) K. Xiong, F. Jiang, Y. Gai, Z. He, D. Yuan, L. Chen, K. Su and M. Hong, *Cryst. Growth Des.*, 2012, **12**, 3335-3341; (m) R. O. Fuller, G. A. Koutsantonis, I. Lozic, M. I. Ogden and B. W. Skelton, *Dalton Trans.*, 2015, **44**, 2132-2137.
- 3 (a) Y. Bi, G. Xu, W. Liao, S. Du, X. Wang, R. Deng, H. Zhang and S. Gao, *Chem. Commun.*, 2010, **46**, 6362-6364; (b) K. Su, F. Jiang, J. Qian, M. Wu, K. Xiong, Y. Gai and M. Hong, *Inorg. Chem.*, 2013, **52**, 3780-3786; (c) Z. Zhang, A. Drapailo, Y. Matvieiev, L. Wojtas and M. J. Zaworotko, *Chem. Commun.*, 2013, **49**, 8353-8355; (d) F.-R. Dai, D. C. Becht and Z. Wang, *Chem. Commun.*, 2014, **50**, 5385-5387; (e) F.-R. Dai, U. Sambasivam, A. J. Hammerstrom and Z. Wang, *J. Am. Chem. Soc.*, 2014, **136**, 7480-7491; (f) K. Su, F. Jiang, J. Qian, Y. Gai, M. Wu, S. M. Bawaked, M. Mokhtar, S. A. Al-Thabaiti and M. Hong, *Cryst. Growth Des.*, 2014, **14**, 3116-3123.
- 4 (a) T. Kajiwara, K. Katagiri, M. Hasegawa, A. Ishii, M. Ferbinteanu, S. Takaishi, T. Ito, M. Yamashita and N. Iki, *Inorg. Chem.*, 2006, **45**, 4880-4882; (b) N. Iki, S. Hiro-oka, M. Nakamura, T. Tanaka and H. Hoshino, *Eur. J. Inorg. Chem.*, 2012, **2012**, 3541-3545, S3541/3541-S3541/3510; (c) N. Iki, S. Hiro-oka, T. Tanaka, C. Kabuto and H. Hoshino, *Inorg. Chem.*, 2012, **51**, 1648-1656.
- 5 C. Feldmann, T. Juestel, C. R. Ronda and P. J. Schmidt, *Adv. Funct. Mater.*, 2003, **13**, 511-516.
- 6 (a) D. T. Palumbo and J. J. Brown, *J. Electrochem. Soc.*, 1970, **117**, 1184-1188; (b) D. T. Palumbo and J. J. Brown, Jr., *J. Electrochem. Soc.*, 1971, **118**, 1159-1164; (c) T. E. Peters, R. G. Pappalardo and R. B. Hunt, Jr., *J. Lumin.*, 1984, **31-32**, 290-292; (d) L. K. Singh, *Indian J. Pure Appl. Phys.*, 1984, **22**, 743-744; (e) B. T. Collins and M. Ling, *J. Electrochem. Soc.*, 1993, **140**, 1752-1755; (f) A. Morell and N. El Khiati, *J. Electrochem. Soc.*, 1993, **140**, 2019-2022; (g) C. Barthou, J. Benoit, P. Benalloul and A. Morell, *J. Electrochem. Soc.*, 1994, **141**, 524-528; (h) L. E. Shea, R. K. Datta and J. J. Brown, Jr., *J. Electrochem. Soc.*, 1994, **141**, 1950-1954.

- 7 (a) H. O. N. Reid, I. A. Kahwa, A. J. P. White and D. J. Williams, *Inorg. Chem.*, 1998, **37**, 3868-3873; (b) H. O. N. Reid, I. A. Kahwa, A. J. P. White and D. J. Williams, *Chem. Commun.*, 1999, 1565-1566; (c) Y. Wei, Y. Yu and K. Wu, *Cryst. Growth Des.*, 2008, **8**, 2087-2089; (d) J. Duan, B. Zheng, J. Bai, Q. Zhang and C. Zuo, *Inorg. Chim. Acta*, 2010, **363**, 3172-3177.
- 8 (a) V. G. Torgov, L. N. Mazalov, G. A. Kostin, T. V. Us, T. M. Korda, N. A. Kryuchkova, E. A. Korotaev, A. D. Fedorenko and A. B. Drapailo, *J. Struct. Chem.*, 2011, **52**, 718-725; (b) N. A. Kryuchkova, S. A. Lavrukina, G. A. Kostin, L. N. Mazalov, V. G. Torgov, A. V. Kalinkin and A. B. Drapailo, *J. Struct. Chem.*, 2013, **54**, 907-916.
- 9 Crystal data. (1): C<sub>96</sub>H<sub>126</sub>FKMn<sub>4</sub>O<sub>34</sub>S<sub>8</sub>, M = 2358.31, Triclinic, P-1, a = 12.0143(9) Å, b = 12.3064(7) Å, c = 18.2691(8) Å, α = 101.431(4)°, β = 99.543(6)°, γ = 90.807(5)°, V = 2607.8(3) Å<sup>3</sup>, R = 0.0521, wR<sub>2</sub> = 0.1015 (I > 2σ(I)).
- 10 L. J. Farrugia, *J. Appl. Crystallogr.*, 2012, **45**, 849-854.
- 11 IGOR PRO v. 6.36, Wavemetrics Inc., Oregon.
- 12 (a) R. Q. Albuquerque, Z. Popovic, C. L. De and G. Calzaferri, *ChemPhysChem*, 2006, **7**, 1050-1053; (b) M. S. Khakhalina, O. A. Rodionova and M. V. Puzyk, *Opt. Spectrosc.*, 2009, **106**, 529-531; (c) M. V. Mina and M. V. Puzyk, *Opt. Spectrosc.*, 2011, **111**, 71-73; (d) C. A. Kent, D. Liu, A. Ito, T. Zhang, M. K. Brennaman, T. J. Meyer and W. Lin, *J. Mater. Chem. A*, 2013, **1**, 14982-14989.
- 13 M. Milos, T. Penhouet, P. Pal and A. Hauser, *Inorg. Chem.*, 2010, **49**, 3402-3408.
- 14 (a) H. G. Drickamer, *Angew. Chem. Int. Ed.*, 1974, **13**, 39-47; (b) J. K. Grey and I. S. Butler, *Coord. Chem. Rev.*, 2001, **219-221**, 713-759.
- 15 S. Sugano, Y. Tanabe, H. Kamimura, *Multiplets of Transition Metal Ions, Pure and Applied Physics*, Vol 33, Academic Press, New York 1970.
- 16 R. Englman and J. Jortner, *Mol. Phys.*, 1970, **18**, 145-164.
- 17 R. Kumar, Y. O. Lee, V. Bhalla, M. Kumar and J. S. Kim, *Chem. Soc. Rev.*, 2014, **43**, 4824-4870.
- 18 N. Iki, H. Kumagai, N. Morohashi, K. Ejima, M. Hasegawa, S. Miyanari and S. Miyano, *Tetrahedron Lett.*, 1998, **39**, 7559-7562.
- 19 N. Morohashi, F. Narumi, N. Iki, T. Hattori and S. Miyano, *Chem. Rev.*, 2006, **106**, 5291-5316.
- 20 CrysAlisPro, Agilent Technologies, Version 1.171.134.149 (release 120-101-2011 CrysAlis2171.NET) (compiled Jan 2020 2011,2015:2058:2025).
- 21 R. C. Clark and J. S. Reid, *Acta Crystallogr., Sect. A: Found. Adv.*, 1995, **51**, 887-897.
- 22 (a) A. Altomare, M. C. Burla, M. Camalli, G. L. Cascarano, C. Giacovazzo, A. Guagliardi, A. G. G. Moliterni, G. Polidori and R. Spagna, *J. Appl. Crystallogr.*, 1999, **32**, 115-119; (b) P. W. Betteridge, J. R. Carruthers, R. I. Cooper, K. Prout and D. J. Watkin, *J. Appl. Crystallogr.*, 2003, **36**, 1487-1487.